IEEE Access
Multidisciplinary ⋮ Rapid Review ⋮ Open Access Journal

Received October 13, 2020, accepted October 25, 2020, date of publication October 28, 2020, date of current version November 10, 2020.

Digital Object Identifier 10.1109/ACCESS.2020.3034436

Design and Implementation of a Germicidal UVC-LED Lamp

FRANCISCO A. JUAREZ-LEON[1], ALLAN GIOVANNI SORIANO-SÁNCHEZ[2], MARTÍN A. RODRÍGUEZ-LICEA[2], AND FRANCISCO J. PEREZ-PINAL[1], (Senior Member, IEEE)

[1]Tecnológico Nacional de México, Instituto Tecnológico de Celaya, Celaya 38010, Mexico
[2]CONACYT, Instituto Tecnológico de Celaya, Celaya 38010, Mexico

Corresponding author: Francisco J. Perez-Pinal (francisco.perez@itcelaya.edu.mx)

This work was supported in part by the Tecnológico Nacional de México, Instituto Tecnológico de Celaya, in part by the Centro de Investigación e Innovación Tecnológica A.C., and in part by the Consejo Nacional de Ciencia y Tecnología (CONACYT) under Grant 4155 and Grant 6782. The work of Francisco A. Juarez-Leon was supported by CONACYT through the M.Sc. Grant.

ABSTRACT In the last years, low pressure ozone UVC mercury germicidal lamps have been widely used to decontaminate air, surfaces, and water. This technology is mature, and it has been widely used during the pandemic as a measure against *SARS-CoV-2*, the coronavirus that causes COVID-19; because the exposure of this virus to the wavelength wave of 254 nm has been proven to be an effective way to eliminate it. However, the Minamata Convention in 2013 decided to limit mercury lamps by 2020; therefore, the development of new technology devices based on UVC-LEDs (short-wave ultraviolet, light-emitting diodes) are receiving a lot of attention. Today, this technology is commercially available from 265 to 300 nm peak wavelengths, and recently up to 254 nm. Notwithstanding, due to the characteristics of these LEDs, arrangements with a precisely dosed power supply are regularly required to provide effective decontamination. Thus, this article reports the design and implementation of a power electronic converter for an array of 254 nm UVC-LEDs, which can be used to decontaminate from *SARS-CoV-2* in a safe way.

INDEX TERMS Control engineering, dc-dc power converters, LED lamps, ultraviolet sources.

I. INTRODUCTION

A germicidal lamp produces short-wave ultraviolet (UVC) light within the 200 to 300 nm range [1]. Until a few years ago, there was only commercially-used low-pressure mercury (LPM) and medium-pressure mercury (MPM) lamps to produce UVC light. An LPM lamp can have an average wavelength of either 185 nm or 254 nm, and it is used to destroy algae, bacteria, fungi, protozoa, and viruses [2]. On the other hand, an MPM has a broad range of 200-600 nm, and it is mainly used for water and surface treatment and advanced oxidation [3]. For those interested in ultraviolet germicidal irradiation, more information can be found in [4].

Some examples of power electronic converters (PECs) developed to drive LPM and MPM lamps can be found in [5]–[9]; such technology is mature, and it has been used widely during the pandemic. For instance, the usage of mercury UVC LPM lamps against COVID-19 and others are listed to follow: application of 0.6–1.0 J/cm^2 of UVC dose for disposable N95 respirators [10]; safety of N95 masks [11]; mobile ''tower'' disinfection device [12]; UVC sterilization of personal protective equipment [13]; disinfection rooms [14].

However, in the Minamata convention on mercury in 2013, a United Nations Environment Program (UNEP), was arranged to forbid, by 2020, mercury-containing merchandises for the well-being of human and environmental health. Nevertheless, mercury UVC lamps are still used for ultraviolet germicidal irradiation (UVGI) systems, and there is still incipient research on replacing them with UVC-LEDs [15]. In 2014, the first deep ultraviolet light-emitting diodes (DUV LEDs) were brought to the market. Early developments were done by Isamu Akasaki and Hiroshi Amano, who had been awarded the Nobel Prize for Physics in December 2014 [16]. UVC-LEDs are monochromatic and available in multiple wavelengths within the germicidal range to attack the invading pathogen, i.e., 255, 265, 275 nm, among others [17].

Today, UVC-LEDs are used in biomedicine, curing, instrumentation, and purification [18]. In this work, a brief review of the state of the art on germicidal UVC-LEDs will follow.

The associate editor coordinating the review of this manuscript and approving it for publication was Eklas Hossain.

An UV LED module, composed of forty 265 nm UVC-LEDs plus a silica lens array, a driver for PWM control, and constant current regulation was reported in [19]. The system was evaluated on controlling four kinds of bacteria and one yeast, for two distances (10 mm, 100 mm) and several exposure times (0 s, 30 s, 60 s, 300 s, and 600 s). The system was able to fully pasteurize the overall bacteria at 600 s at both distances, but it failed for yeast. To overcome this limitation, authors recommended: increasing the exposure time, using an array of different UVC wavelengths or improving the silica lens.

An UVC-LEDs disinfection system for mycobacterium tuberculosis was reported in [20]. Ten Crystal IS's LEDs of different wavelengths were selected and evaluated to design the proposed system. Results regarding UV flux versus consumed current, wavelength spectral distribution, and disinfection rate at two humidity levels were reported. Unfortunately, no information about PEC used to drive the UVC-LEDs was reported.

The use of an UVC-LED array in a chamber-type air disinfection system was reported in [21]. In this article, the inactivation of aerosolized viruses, bacteria, and fungi was studied. Sixteen UVC-LED package chips from LG Innotek Co. were connected and arrayed linearly on printed circuit boards (PCBs). A distance of 11 mm between UVC-LEDs was given, and 40 mm of blank space on both sides was provided for cooling; 12 V, 1.6 A were applied to the UVC-LED array. Authors concluded that UVC-LED can effectively inactivate microorganisms regardless of taxonomic classification, and it can substitute conventional mercury UV lamps. Unfortunately, no information about the used PEC was reported.

A wearable device based on an adjustable UVC-LED lamp, a camera, and a mobile application for onychomycosis treatment was reported in [22]; unfortunately, no further details about this design was found in the major databases. An array of three UVC-LED manufactured by Seoul VIOSYS (CA3535-CUD7GF1A) was used to develop a germicidal system in [23]. The system comprised three sections: an automatic constant current control module, an automatic electric power control module, and an automatic power control module. Irradiation experiments were done for three types of bacteria (Acinetobacter baumannii, Staphylococcus aureus, and Escherichia coli). Different inputs (illumination height, illumination time, temperature, and strain concentration), and different outputs (sterilization dose, sterilization residual amount and dose distribution, optimal sterilization distance, sterilization shortest time, sterilization mortality rate, sterilization parameter factor optimal configuration, and minimum bactericidal dose) were reported. The system was able to eliminate the bacteria, but no information about the developed PEC was reported.

An interesting comparison between performance of pulsed and continuous UVC-LED for the E. coli bacteria inactivation was reported in [24]. It was also reported that both techniques provide similar inactivation efficiency. However, it was noticed that an increment of ambient temperature and driving current in the UVC-LED increased the solder temperature, which had a negative impact on the wavelength, optical power and irradiance. Therefore, an accurate frequency and a specific duty cycle to drive UVC-LEDs was suggested. Unfortunately, a Yokogawa S610 programmable voltage/current source was used as a power source, and the PEC design was omitted.

UVC-LEDs within the 200-280 nm range for disinfection of Bacillus species and their tetracycline resistant gene (TRG) in water was reported in [25]. Results indicated that UVC-LEDs were able to inactivate TRB and inhibit TRG at 268 nm wavelength. But, once again, information about the PEC used to drive the UVC-LED arrangement was not given. A comparison between UVC-LEDs and conventional UVGI system was reported in [14] for room air disinfection. Ten UVC-LEDs (Klaran series, Crystal IS Inc.) with a wavelength of 254 nm were arranged in a 5×2 matrix with a rated voltage and current of 9 V and 3.5 A, respectively. The UVC-LED system was tested with three different bacteria, different input currents (irradiation levels), different times, and continuous currents. A linear relationship between the input current and intensity was found up to 43% of the rated current, after this level, no significant changes in intensity was reported even with an increment of the input current. The UVC-LEDs were able to reduce the indoor microbial concentration but, according to the authors, this minimization varies depending on the bacteria type. Again, information about the used PEC to drive the UVC-LED was not reported.

To summarize the above paragraphs, low pressure mercury lamps are expected to be discontinued soon, and UVC-LEDs are an environmentally friendly replacement. However, to the best authors' knowledge, only marginal information about the power electronic converters and controllers designed for an array of UVC-LEDs has been reported.

Therefore, this article proposes a Ćuk converter as a main power source for this kind of application. Section II reports the general consideration to design the PEC, in this work a deep ultraviolet light-emitting diode with peak emission wavelengths from 250 nm to 260 nm (CUD5GF1B) from SEOUL VIOSYS as a main UVC-LED was chosen. Practical results in an array of 5×2 matrix are reported in Section III. It is necessary to mention that the above parameters influence the UVC-LED wavelength, efficiency and the relative spectral power. In Section IV, a discussion about recent reports regarding UVC-LED technology is provided. Likewise, applications of the proposal to different UVC-LED wavelengths are also included. Finally, a summary of the proposed system and future research directions are given in the final section of this manuscript.

II. CONVERTER DESIGN

A. PRELIMINARIES

UVC-LEDs have characteristics in common with LEDs, i.e.: nominal DC current, varying voltage depending on the LED

arrangement, and being are environmentally friendly [26]. Today, it can be found in literature, linear power regulators or several PECs, which can be applied to UVC-LEDs, for instance: non-isolated/isolated, unidirectional/bidirectional, voltage-fed/current-fed, hard switched/soft switched, and minimum/non-minimum phase controller configuration. An interesting review about step up converters can be found in [27], but this conclusion can be extended to step-down or step-up and down converters. The selection of a PEC for an UVC-LEDs array is based on several factors, including: complexity, cost, efficiency, integration, power density, power level, weight, and reliability [28]. Additionally, LEDs limitations are: lifetime expectation in terms of temperature, addition of devices not as reliable as LEDs; and it is expected that PECs applied to UVC-LEDs would have similar characteristics. For instance, an isolated PEC design for a LEDs lamp is reported in [29]. A comparison of PECs for UVC-LEDs based on the previous paragraphs is out of the scope of this article, and to the best knowledge of the authors, it is open for researching. In this article, a two-stage PEC configuration was selected: a typical AC/DC rectifier with power factor correction (PFC), and a lamp driver as shown in Fig. 1.

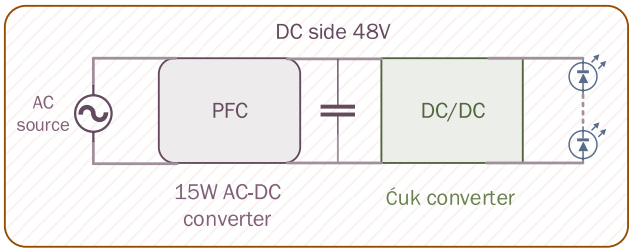

FIGURE 1. Two stage AC, UVC-LED driver.

The first stage consists of a conventional EMI filter, a rectifier, a power factor corrector, and a capacitor. For this stage, a commercial 15 W AC/DC power supply was selected: PSA15R-480P6-R, 90-254 VAC input voltage, and 48 V output voltage. The second stage consists of a Ćuk converter operating in continuous conduction mode (CCM) [30], [31]. The latter was selected because the input and output currents are continuous (compared to other topologies, such as: BUCK/BOOST, SEPIC or ZETA), which reduces the EMI filter requirements, the switching stress, among other characteristics. Details about the mathematical model, steady-state and design equations of the Ćuk converter can be found in Appendix A.

B. COMPONENT SELECTION

The selected UVC-LED CUD5GF1B, according with its datasheet, has an adequately operating point at 100 mA at 7.5 V [32]. The proposed array is composed by ten LEDs connected in series; this means, a voltage of 75 V will be required. On the other hand, for the Ćuk converter (Fig. 2),

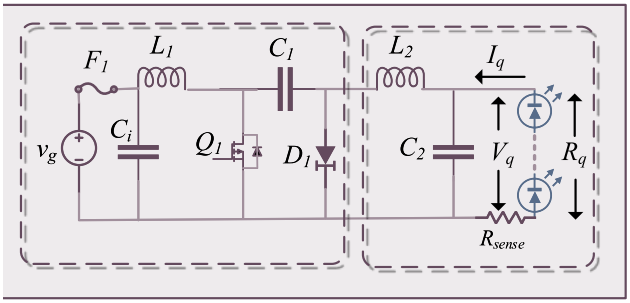

FIGURE 2. Ćuk converter.

an input voltage of 48 V has been proposed. As can be seen, the LED array current is measured with a current-sense resistor R_{sense}.

Therefore, the following design parameters must be considered: input voltage: $V_g = 48$ V, voltage of the LED array: $V_q = 75$ V, LED array's power consumption: $P_q = 7.5$ W, current of the LED array: $I_q = 100$ mA, equivalent resistance of the LED array: $R_q = V_q/I_q = 750\ \Omega$, current-sense resistor: $R_{sense} = 5.6\ \Omega$, voltage across the current-sense resistor: $V_{sense} = R_{sense}I_q = 560$ mV, total load resistance: $R_o = R_q + R_{sense} = 755.6\ \Omega$, output voltage: $|V_o| = |V_{C_2}| = V_q + V_{sense}$, and switching frequency: $f_{sw} = 200$ kHz. In the case of R_{sense}, this resistor does not drastically increase the value of R_o, so that both the overall efficiency is not compromised and the voltage drop across R_{sense} is appropriate for the control scheme. Assuming ideal components in the PEC, the corresponding duty cycle can be calculated as follows:

$$D = \frac{|V_o|}{|V_o| + V_g} = \frac{75.56}{75.56 + 48} = 0.6115 \tag{1}$$

Likewise, according to "(25)" and considering the design parameters, steady-state values of the PEC will be:

$$\vec{X} = \begin{bmatrix} I_{L_1} \\ I_{L_2} \\ V_{C_1} \\ V_{C_2} \end{bmatrix} = \begin{bmatrix} 157.42\ mA \\ -100\ mA \\ 123.56\ V \\ -75.56\ V \end{bmatrix}$$

As can be seen, the inductor currents are considerably small and for that reason, commercial-SMD inductors can be used in the converter. The next design step is to determine the value of inductors and capacitors considering the following current and voltage ripple specifications:

- Inductor 1 - Current ripple: $\Delta_1 = 0.15I_{L_1} = 23.61$ mA
- Inductor 2 - Current ripple: $\Delta_2 = 0.15I_{L_1} = -15$ mA
- Capacitor 1 - Voltage ripple: $\delta_1 = 0.05V_{C_1} = 6.178$ V
- Capacitor 2 - Voltage ripple: $\delta_2 = 0.0015V_{C_2} = -113.34$ mV

Thus, the inductors and capacitors values can be calculated as follows "(26)"-"(29)":

$$L_1 = \frac{V_g D}{2\Delta_1 f_{sw}} = \frac{(48)(0.6115)}{(2)(0.02361)(200\times10^3)} = 3.1\ mH$$
$$L_2 = -\frac{V_g D}{2\Delta_2 f_{sw}} = \frac{-(48)(0.6115)}{(2)(-0.015)(200\times10^3)} = 4.89\ mH$$
$$C_1 = -\frac{I_{L_2} D}{2\delta_1 f_{sw}} = -\frac{(-0.1)(0.6115)}{(2)(6.178)(200\times10^3)} = 24.74\ nF$$
$$C_2 = \frac{\Delta_2}{8 f_{sw}\delta_2} = \frac{-0.015}{(8)(200\times10^3)(-0.11334)} = 82.71\ nF$$

For the inductors, in order to have a single part number, both inductances would be equal to 4.7 mH. The fixed inductor MSS1210-475KED is a part number from Coilcraft, with an inductance of 4.7 mH ± 10%, 490 mA and a typical series resistance of 3.34 Ω. In the case of the capacitor C_1, the capacitance has been established in 22 nF. Thus, the selected commercial number is C1206C223JAGACTU. This capacitor can handle a maximum DC voltage of 250 V, with a 5% tolerance and a negligible ESR. Capacitor C_2 would be set to 100 nF. The selected part number is C3216 × 7R2E104K. Likewise, the selected switch is a MOSFET IPN60R360P7SATMA1 from Infineon Technologies. This device can handle a maximum drain-source voltage of 650 V and a continuous drain current of 9 A (at 25°C); also, it has 360 mΩ resistance when it is turned on. Finally, for the diode, a BAV21W-E3-08 form Vishay Technologies was selected. The forward voltage of this diode, V_D is equal to 1 V. Therefore, once the passive and active devices have been selected, the parasitic elements will be:

$$\begin{cases} R_{L_1} = R_{L_2} = 3.34\,\Omega \\ R_{C_1} = 0\,\Omega \\ R_{on} = 0.36\,\Omega \\ V_D = 1\,V \end{cases}$$

Considering these non-ideal parameters and solving for the "real" duty cycle, it increases slightly to 0.61883. Thus, solving numerically "(23)", it yields to:

$$\vec{X} = \begin{bmatrix} I_{L_1} \\ I_{L_2} \\ V_{C_1} \\ V_{C_2} \end{bmatrix} = \begin{bmatrix} 162.35\ mA \\ -100\ mA \\ 123.35175\ V \\ -75.56\ V \end{bmatrix}$$

Comparing the ideal solution with the "real" solution, it can be seen that there is not too much difference in the steady-state values. On the other hand, the vector $\vec{J}$ "(31)" will be:

$$\vec{J} = \begin{bmatrix} 124.25731 \\ -124.25731 \\ -0.26235 \\ 0 \end{bmatrix}$$

These two vectors will be useful to properly determine the controller of the PEC.

C. CONTROLLER DEVELOPMENT

Evaluating the 4th-order transfer function of "(34)", it yields to:

$$\frac{\hat{V}_{sense}(s)}{\hat{d}(s)} = \frac{b_2 s^2 + b_1 s + b_0}{a_4 s^4 + a_3 s^3 + a_2 s^2 + a_1 s + a_0} \tag{2}$$

where the numerical coefficients are:

$$b_2 = -7.195\times10^{-8}$$
$$b_1 = 0.004222$$
$$b_0 = -261.9$$
$$a_4 = 3.672\times10^{-17}$$
$$a_3 = 5.417\times10^{-13}$$
$$a_2 = 2.665\times10^{-7}$$
$$a_1 = 0.002692$$
$$a_0 = 111.8$$

Fig. 3 shows the closed control loop scheme proposed for the Ćuk converter. Due to the change of polarity of the output voltage, it is necessary to add an inverter voltage with unitary gain. The transfer function $H(s)$ is an optional low-pass filter, which can be added to minimize the high-frequency voltage ripple in the feedbacked signal, $F(s)$ represents the transfer function of a "soft-start" stage, $G_c(s)$ the controller transfer function, and V^*_{sense} the voltage reference that determines the desired voltage across the current-sense resistor.

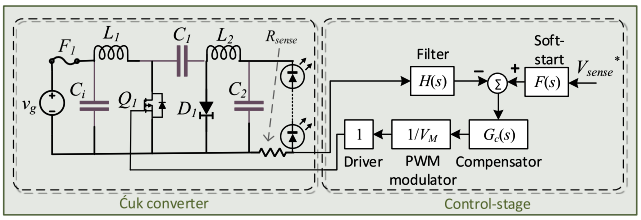

FIGURE 3. Control loop scheme.

In addition, in the control scheme V_M is the amplitude of the sawtooth signal, generated by the PWM modulator inside the TL494, which has a value of 3 V. Thus, it is possible to determine the "loop gain", which can be defined as the products of the gains around the forward and feedback paths of the loop [33].

$$T(s) = -1\frac{\hat{V}_{sense}(s)}{\hat{d}(s)} H(s)\frac{1}{V_M} G_c(s) \tag{3}$$

Initially, the controller $G_c(s)$ will be equal to 1, it means, there will not be any type of control action with the aim of determine the stability characteristics of the PEC: the phase and gain margins. Evaluating $T(s)$ without a controller and without filtering ($H(s) = 1$):

$$T_{uncomp}(s) = \frac{c_2 s^2 + c_1 s + c_0}{a_4 s^4 + a_3 s^3 + a_2 s^2 + a_1 s + a_0} \tag{4}$$

where the numerical coefficients are:

$$c_2 = 2.398\times10^{-8}$$

$$c_1 = -0.001407$$
$$c_0 = 87.29$$

Fig. 4 shows the Bode diagram of the uncompensated loop gain $T_{uncomp}(s)$. As can be observed, the PEC without controller has a phase margin of 150° and a gain margin of 3.96 dB. In order to assure the zero steady-state error, an integral action must be added at low frequency. Thus, an inverted zero can be used (PI-controller) "(5)":

$$G_c(s) = K_z \frac{s + \omega_z}{s} \tag{5}$$

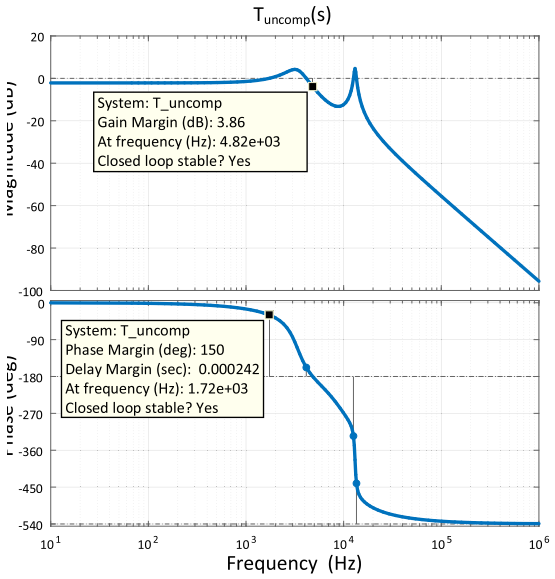

FIGURE 4. Bode diagram of $T_{uncomp}(s)$.

By selecting $K_z = 0.25$ and $\omega_z = 19000$ rad/s, and computing again "(3)", the compensated loop gain $T_{comp}(s)$ will be:

$$T_{comp}(s) = \frac{d_3 s^3 + d_2 s^2 + d_1 s + d_0}{s\left(a_4 s^4 + a_3 s^3 + a_2 s^2 + a_1 s + a_0\right)} \tag{6}$$

with:

$$d_3 = 5.996 \times 10^{-9}$$
$$d_2 = -0.0002379$$
$$d_1 = 15.14$$
$$d_0 = 4.146 \times 10^{5}$$

Thus, the gain margin will be 7.89 dB and the phase margin 92.4°, as shown in Fig. 5. Likewise, the crossover frequency f_c occurs at 621 Hz. For this type of application, it is not necessary to have a large bandwidth because the load does not change drastically. Finally, Fig. 6 shows the physical implementation of the proposed system. As can be seen, the Ćuk converter has dimensions of 5 × 3 cm. In addition, the schematic of this PEC can be consulted in Appendix B.

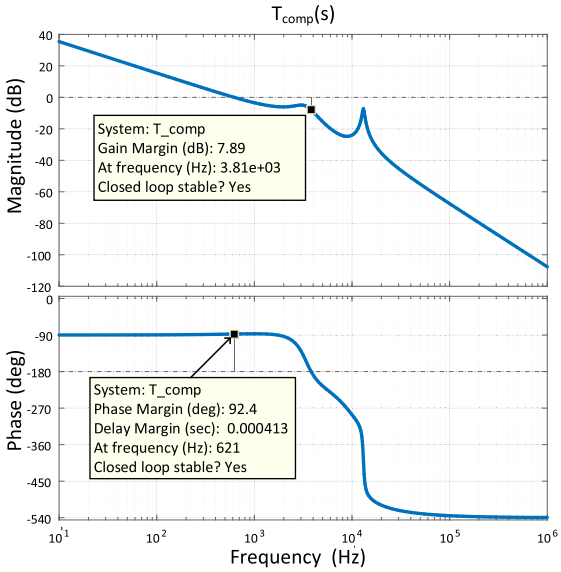

FIGURE 5. Bode diagram of $T_{comp}(s)$.

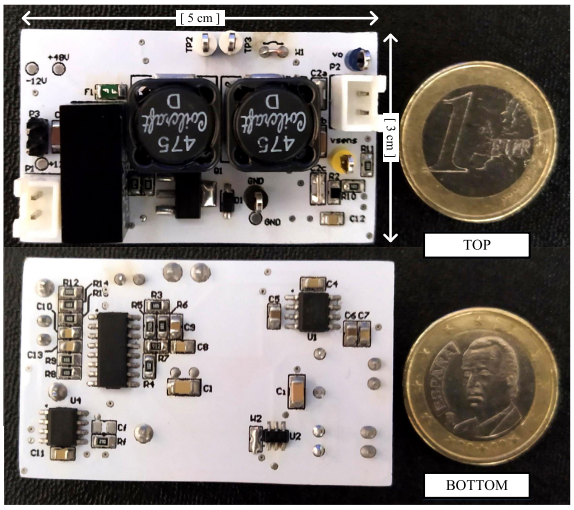

FIGURE 6. Practical converter, top and bottom views.

III. EXPERIMENTAL RESULTS

Fig. 7 provides the results obtained from soft-start. As shown in this figure, the system achieves steady state in less than two seconds, which is more than enough for the lamp application. It can be also noted that the system provides the rated current of 100 mA at approximately 68 V. This is an unexpected outcome because the manufacturer's datasheet reported a rated voltage per UVC-LED of 7.5 V (total voltage of 75 V). Because LEDs are constant current devices, the reference voltage V^*_{sense} was adjusted to achieve the rated current and avoiding damaging the UVC-LEDs array. It is important to note that during shutdown, the Ćuk converter evades a possible leakage current through the LEDs because the system is not directly connected to ground.

On the other hand, Fig. 8 shows the transistor and diode voltages during transitions. These results are in line with

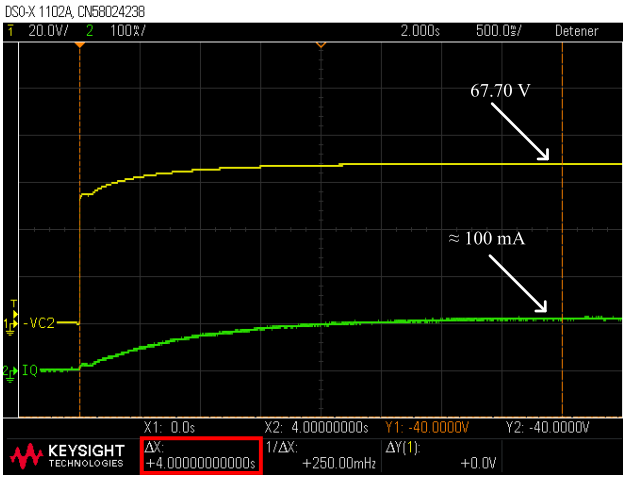

FIGURE 7. Soft-start.

FIGURE 9. Steady-state inductor currents.

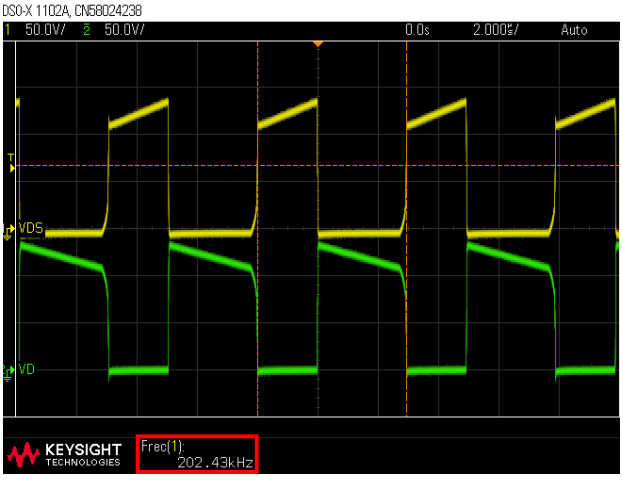

FIGURE 8. Transistor and diode voltages.

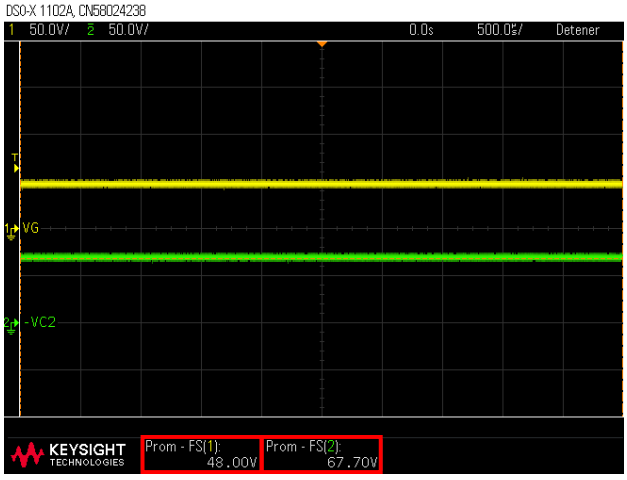

FIGURE 10. Steady-state input and output voltages.

those reported in previous studies, where the turn on/off commutation behaves as expected. In addition, by analyzing these waveforms, it can be observed that the PEC is operating in CCM, despite the fact of the unexpected outcome previously mentioned.

Fig. 9 displays the steady-state currents through inductors L_1 and L_2, with average values of 164.46 mA and -106.54 mA, respectively. These values slightly differ with those obtained in the design stage. Similarly, Fig. 10 shows the input and output voltages, v_g and v_{C_2}, respectively. The first one has a nominal average value of 48 V, while the second one, an average value of -67.7 V (considering the polarity shown in Fig. 15). Finally, the total current demanded by the whole circuit (including the power and control stages) and the LED array current are shown in Fig. 11. Indeed, the practical efficiency can be also calculated from these figures. The power-stage would have an efficiency of:

$$\eta_{\acute{C}uk} = \frac{-V_{C_2} \times I_q}{I_{L_1} \times V_g} = \frac{(67.7)\,(0.10691)}{(0.16446)\,(48)} = 0.9169 \quad (7)$$

Likewise, the overall efficiency of the designed circuit would be:

$$\eta_{total} = \frac{-V_{C_2} \times I_q}{I_{in} \times V_g} = \frac{(67.7)\,(0.10691)}{(0.18046)\,(48)} = 0.8355 \quad (8)$$

It is important to notice that this last efficiency can be considered low compared to high power density PEC. The main reason for this is because the control-stage and the driver-stage of the PEC requires a voltage of ± 12 V to operate. For that purpose, a commercial low power DC/DC converter was used, as can be seen in Fig. 6. Notwithstanding, the efficiency of the power-stage is considerably high (taking into account the parasitic elements and the high-switching frequency). Finally, a thermal capture is used to illustrate how the proposed design behaves on steady state (Fig. 12).

IV. GERMICIDAL PROPERTIES

As mentioned above, the main motivations to develop germicidal UVC-LED lamps are based on two aims: firstly, the Minamata convention agreements, and recently,

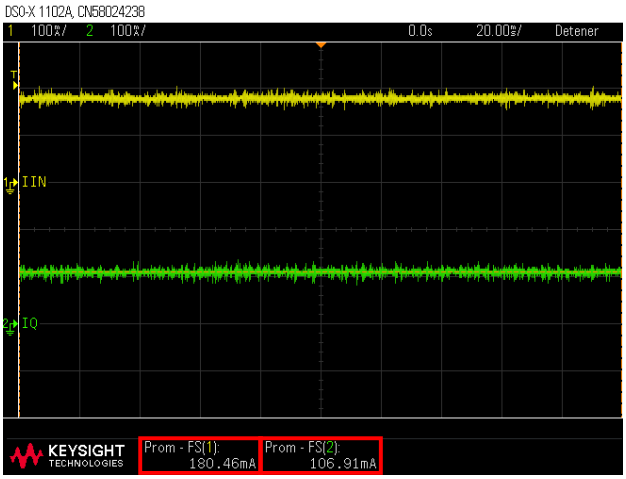

FIGURE 11. Steady-state input and output currents.

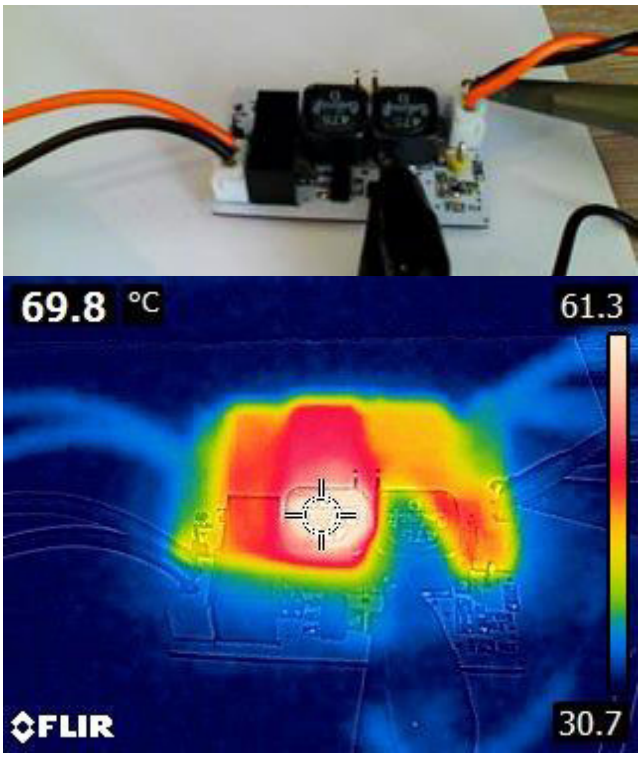

FIGURE 12. Ćuk converter - Thermal capture.

the *SARS-CoV-2*. According to [10], the literature supports that UVC exposures of 1 J/cm^2 are capable of decontaminating influenza virus and *SARS-CoV-2* in N95 filter mask respirators. Additionally, research has shown that exposures as low as 2-5 mJ/cm^2 are capable of inactivating coronaviruses on surfaces. The UVC dose is calculated based on the standard method for mathematical modeling of UV-light using the following equation [34]:

$$UV_{dose}\left(\frac{J}{cm^2}\right) = Irradiance\left(\frac{W}{cm^2}\right) \times Time(s) \qquad (9)$$

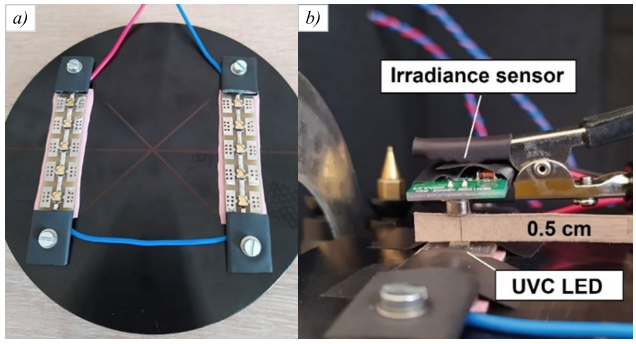

FIGURE 13. UVC-LED array and emitting tests.

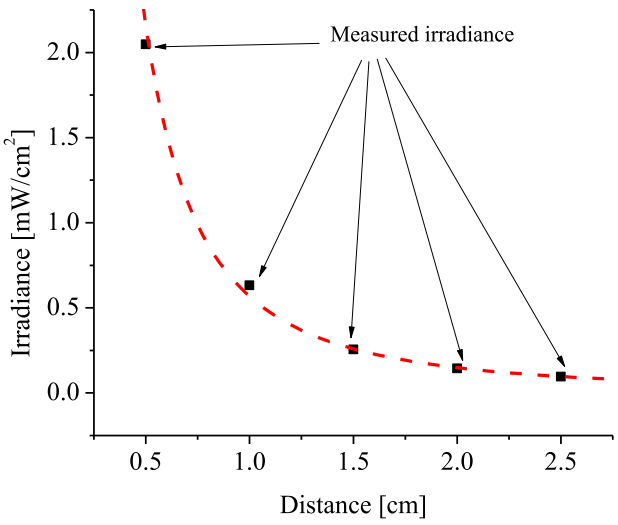

FIGURE 14. Irradiation experimental results.

where UV_{dose} is the radiation dose required in Joules per square centimeter, *Irradiance* is the radiation emitted by the source in Watts per square centimeter, and *Time* is the time in seconds required to eliminate the virus. Fig. 13a) shows the arrangement of 10 UVC-LEDs of the type CUD5GF1B from the company SEOUL VIOSYS. This array of LEDs is mounted on a 130 × 30 mm heat sink from the Wakefield-Vette brand. Fig. 13b) shows the UVC-LED sensor (top) evaluating the irradiation at 0.5 cm from the UVC-LED. The sensing module is a GUVC-T10GM-LA of the Genicom Co., Ltd. brand, which is capable of measuring from 0 to 20 mW/cm^2 and produces a linear output from 0 to 5 V. In addition, Fig. 14 shows the irradiation curve evaluated to one UVC-LED. The developed prototype delivers a maximum radiation power of 2 mW/cm^2 at 0.5 cm and drops to 0.2 mW/cm^2 at 2.5 cm.

Applying "(9)" to the developed prototype, it would be necessary to expose the *SARS-CoV-2*, at 0.5 cm, 500 seconds to the UVC-LED system developed to eliminate it. Please note that the exposure time will vary depending on the distance between the emitting UVC-LED and the receiving entity. It is important to mention that the reported system

behaves similarly to the system developed by researchers at the Ferdinand Braun Institute in Germany and the Technical University of Berlin [35]. Accordingly, with authors, the system contains a matrix of 118 UVC-LEDs spread over an area of 64 cm^2 and emitting UVC light at a wavelength of around 230 nm. The configuration provides a maximum irradiance power of 0.2 mW/cm^2 over an area of 36 cm^2, with 90% uniformity. Applying "(9)" to reported data [35], one would need to expose *SARS-CoV-2*, 500 seconds to the UVC-LED system to eliminate it, which agrees with calculation of the proposed system. Today, international efforts are ongoing to test different UVC-LED wavelengths, time and distance to eliminate the *SARS-CoV-2*. Future applications of the developed systems include water, surfaces, and air decontamination, as well as chamber air disinfection systems, among others. At the beginning of this research, tests reported in the literature showed that ozone-based germicidal lamps with a wavelength of 254 nm eliminate *SARS-CoV-2*.

However, it has been recently reported that other UV wavelengths can deactivate the virus. For instance, a new study published in June 2020 by researchers from the Columbia University Irving Medical Center reported that more than 99.9% of seasonal coronaviruses, present in air droplets, died when exposed to distant UVC-light (222 nm) [36]. In addition, a study published in July 2020, by researchers from the Nikkiso company in Tokyo Japan [37], reported that a 280±5 nm wavelength deep ultraviolet light-emitting diode (DUV LED) rapidly inactivates the *SARS-CoV-2* obtained from a patient with COVID-19. It was not reported in the original manuscript specifications regarding this DUV, but after research, it was found that it agrees to a VPS 164-280 second generation, which has a wavelength of 280±5 nm, 500 mA, 40 mW, 6 V. This DUV LED is a miniature surface mount (SMD) device in a 3.5 mm square package [38].

Likewise, another study published in July 2020 [39], reported that an array of five LEDs with a maximum wavelength of 343±3 nm placed 1 cm above the plate inactivated various pathogens, including coronavirus-229E. Once again, a quick research was done to determine the DUV's characteristics, and it was found that it corresponds to a CUD4AF1B, which has a wavelength of 343±3 nm, 700 mA, 55 mW, 4.3 V. This DUV LED is a miniature surface mount (SMD) device in a 6.35 × 6.355×1.8 mm package [40]. It can be noticed from [32], [38] and [40] similar characteristics in power consumption, voltage, and current from the different UV LED wavelengths. Indeed, only the optical output power significantly varies from 7 mW to 55 mW. Table 1 summarizes data for the Ćuk converter design reported in this article and extended to these different UVC-LED arrays.

TABLE 1. Application of Ćuk Converter for different UV LEDs.

Parameter	CUD5GF 1B [32]	VPS 164-280 [38]	CUD4AF 1B [40]
Wavelength	254 nm	280 nm	343 nm
Voltage per LED	7.5 V	6 V	4.3 V
LED current	100 mA	500 mA	700 mA
LED equiv. resistance	75 Ω	12 Ω	6.14 Ω
Optical output power (max)	7 mW	40 mW	55 mW
Number of LEDs arrangement	10	15	20
Total voltage	75 V	90 V	86 V
Total equiv. resistance	750 Ω	180 Ω	122.85 Ω
Total power	7.5 W	45 W	60.2 W
L_1	4.7 mH	556 μH	410 μH
L_2	4.7 mH	1.2 mH	740 μH
C_1	22 nF	120 nF	167 nF
C_2	100 nF	470 nF	510 nF

V. CONCLUSION

This article provides a step-by-step modeling, design, and implementation of a Ćuk converter as a main source to supply a UVC-LEDs lamp. The converter works in CCM supplying continuous input and output current to reduce switching stress. Practical results of the converter and performance evaluations during different tests are also reported. Additionally, experimental evaluation of the UVC dose is calculated based on the standard method for mathematical modeling of UV-light. This latter is an essential parameter to measure the effectiveness of decontaminating several entities from *SARS-CoV-2* in a safe and easy way. Finally, the extension of this converter to other UV LED arrangements proven to deactivate different viruses is also given.

APPENDIX A
Ćuk CONVERTER MODELLING

With the aim of obtaining a very precise mathematical description of the proposed PEC, the state-space averaging technique was used. This mathematical tool approximates a variable structure system (which naturally is a non-linear system) to a continuous-time linear system, with the advantage of a formal mathematical notation. It is straightforward to determine voltage and currents in steady-state and finding the transfer functions that describe the dynamic behavior of the converter [41].

Particularly, for the Ćuk converter the state vector $\vec{x}(t)$ has four variables: two for the inductor currents (i_{L_1} and i_{L_2}) and two for the capacitor voltages (v_{C_1} and v_{C_2}) "(10)". On the other hand, the input vector $\vec{u}(t)$, will have two variables: the input voltage $v_g(t)$ and the nominal forward voltage of the diode V_D "(11)". Also, for this application, the converter will be operating in CCM, that means, inductor currents will be different from zero along the two operating intervals depending on the state of the main switch: t_{on} and t_{off}.

$$\vec{x}(t) = \begin{bmatrix} i_{L_1}(t) \\ i_{L_2}(t) \\ v_{C_1}(t) \\ v_{C_2}(t) \end{bmatrix} \tag{10}$$

$$\vec{u}(t) = \begin{bmatrix} v_g(t) \\ V_D \end{bmatrix} \tag{11}$$

In addition, the system's constants matrix needs to be defined as follows:

$$K = \begin{bmatrix} L_1 & 0 & 0 & 0 \\ 0 & L_2 & 0 & 0 \\ 0 & 0 & C_1 & 0 \\ 0 & 0 & 0 & C_2 \end{bmatrix} \tag{12}$$

As can be seen, this matrix includes the values of inductances and capacitances of the proposed converter.

A. t_{on} INTERVAL

The equivalent circuit of the converter in t_{on} interval is shown in Fig. 15. Analyzing the converter in this interval, the following state-space equation is obtained:

$$K\frac{d}{dt}\vec{x}(t) = A_1\vec{x}(t) + B_1\vec{u}(t) \tag{13}$$

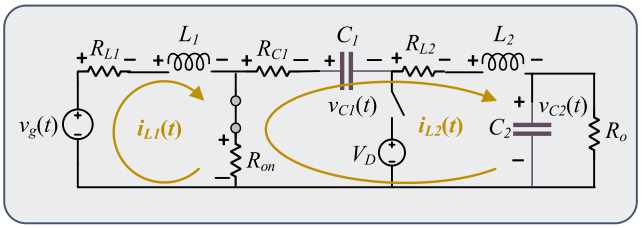

FIGURE 15. Ćuk converter, t_{on} interval.

where the state matrix A_1 and the input matrix B_1 are:

$$A_1 = \begin{bmatrix} \alpha_1 & R_{on} & 0 & 0 \\ R_{on} & \beta_1 & -1 & -1 \\ 0 & 1 & 0 & 0 \\ 0 & 1 & 0 & -\frac{1}{R_o} \end{bmatrix} \tag{14}$$

$$B_1 = \begin{bmatrix} 1 & 0 \\ 0 & 0 \\ 0 & 0 \\ 0 & 0 \end{bmatrix} \tag{15}$$

with $\alpha_1 = -R_{L_1} - R_{on}$ and $\beta_1 = -R_{on} - R_{L_2} - R_{C_1}$.

B. t_{off} INTERVAL

Fig. 16 shows the equivalent circuit of the Ćuk converter in t_{off} interval. Analyzing the converter in this interval, the following state-space equation is obtained:

$$K\frac{d}{dt}\vec{x}(t) = A_2\vec{x}(t) + B_2\vec{u}(t) \tag{16}$$

where the state matrix A_2 and the input matrix B_2 are:

$$A_2 = \begin{bmatrix} -R_{L_1} - R_{C_1} & 0 & -1 & 0 \\ 0 & -R_{L_2} & 0 & -1 \\ 1 & 0 & 0 & 0 \\ 0 & 1 & 0 & -\frac{1}{R_o} \end{bmatrix} \tag{17}$$

$$B_2 = \begin{bmatrix} 1 & -1 \\ 0 & 1 \\ 0 & 0 \\ 0 & 0 \end{bmatrix} \tag{18}$$

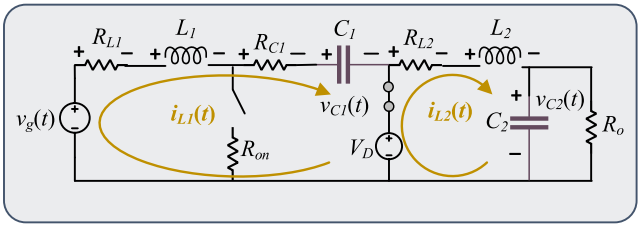

FIGURE 16. Ćuk converter, t_{off} interval.

C. AVERAGED MODEL

Once the state-space equation of each interval has been obtained "(13)" and "(16)", it is possible to combine them in an averaged state-space equation:

$$K\frac{d}{dt}\vec{x}(t) = A_P\vec{x}(t) + B_P\vec{u}(t) \tag{19}$$

where matrices A_P and B_P can be determined as follows:

$$\begin{aligned} A_P &= A_1D + A_2(1-D) \\ B_P &= B_1D + B_2(1-D) \end{aligned} \tag{20}$$

with the variable D as the steady-state duty cycle. Replacing matrices A_1, A_2, B_1, and B_2 in the previous equations, the following averaged matrices are obtained:

$$A_P = \begin{bmatrix} \alpha_P & DR_{on} & D-1 & 0 \\ DR_{on} & \beta_P & -D & -1 \\ \text{1-D} & D & 0 & 0 \\ 0 & 1 & 0 & -\frac{1}{R_o} \end{bmatrix} \tag{21}$$

$$B_P = \begin{bmatrix} 1 & D-1 \\ 0 & 1-D \\ 0 & 0 \\ 0 & 0 \end{bmatrix} \tag{22}$$

with $\alpha_P = DR_{C_1} - R_{L_1} - DR_{on} - R_{C_1}$ and $\beta_P = -R_{L_2} - DR_{on} - DR_{C_1}$.

D. STEADY-STATE SOLUTION AND DESIGN EQUATIONS

From the averaged model "(19)" it is possible to determine the steady-state solution as follows [33]:

$$\vec{X} = -A_P^{-1}B_P\vec{U} = \begin{bmatrix} I_{L_1} & I_{L_2} & V_{C_1} & V_{C_2} \end{bmatrix}^T \tag{23}$$

Due to the parasitic elements, the analytical solution of this equation can be large and complex. Notwithstanding, the numeric solution can be computed easily. For design purposes, the first approach needs to be done with ideal elements, that means, all the parasitic elements will be considered equal to zero:

$$\begin{cases} R_{L_1} = R_{L_2} = R_{C_1} = R_{on} = 0\,\Omega \\ V_D = 0\,V \end{cases} \tag{24}$$

Solving "(23)" with the previous considerations, the ideal solution is given by:

$$\vec{X} = \begin{bmatrix} \frac{V_g}{R_o}\left(\frac{D}{1-D}\right)^2 \\ -\frac{V_g}{R_o}\left(\frac{D}{1-D}\right) \\ V_g\left(\frac{1}{1-D}\right) \\ -V_g\left(\frac{D}{1-D}\right) \end{bmatrix} \tag{25}$$

Likewise, by using current and voltage equations (either the equations of t_{on} or t_{off}), design equations can be derived. These equations will be in function of the operating point, the current and voltage ripples on each inductor and capacitor, respectively, and they can be used to determine the inductances and capacitances that assure the CCM operation in the PEC "(26)"-"(29)":

$$L_1 = \frac{V_g D}{2\Delta_1 f_{sw}} \tag{26}$$

$$L_2 = -\frac{V_g D}{2\Delta_2 f_{sw}} \tag{27}$$

$$C_1 = -\frac{I_{L_2} D}{2\delta_1 f_{sw}} \tag{28}$$

$$C_2 = \frac{\Delta_2}{8 f_{sw} \delta_2} \tag{29}$$

where Δ_1 is the current ripple in L_1, Δ_2 the current ripple in L_2, δ_1 the voltage ripple in C_1, δ_2 the voltage ripple in C_2, and f_{sw} the switching frequency.

E. SMALL SIGNAL MODEL

From the obtained averaged state-space model of the Ćuk converter "(19)", a "perturbed" model can be derived. This new model can describe the system's dynamic under small AC perturbations in the state variables, input variables, and control signal. Thus, this model is given by the next equation:

$$K\frac{d}{dt}\hat{x}(t) = A_P\hat{x}(t) + B_P\hat{u}(t) + \vec{J}\hat{d}(t) \tag{30}$$

where the vector $\vec{J}$ is a vector that depends on the operating point and can be calculated as follows:

$$\vec{J} = (A_1 - A_2)\,\vec{X} + (B_1 - B_2)\,\vec{U} \tag{31}$$

Applying the Laplace Transform to "(30)", it yields to:

$$sK\hat{X}(s) = A_P\hat{X}(s) + B_P\hat{U}(s) + \vec{J}\hat{d}(s) \tag{32}$$

Neglecting the "perturbed" input vector $\hat{U}(s)$, the control-to-output transfer functions can be obtained:

$$\frac{\hat{X}(s)}{\hat{d}(s)} = (sK - A_P)^{-1}\vec{J} = \begin{bmatrix} \frac{\hat{I}_{L_1}(s)}{\hat{d}(s)} & \frac{\hat{I}_{L_2}(s)}{\hat{d}(s)} & \frac{\hat{V}_{C_1}(s)}{\hat{d}(s)} & \frac{\hat{V}_{C_2}(s)}{\hat{d}(s)} \end{bmatrix}^T \tag{33}$$

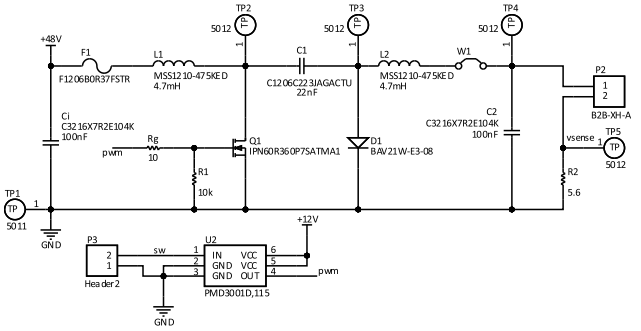

FIGURE 17. Power and driver stages.

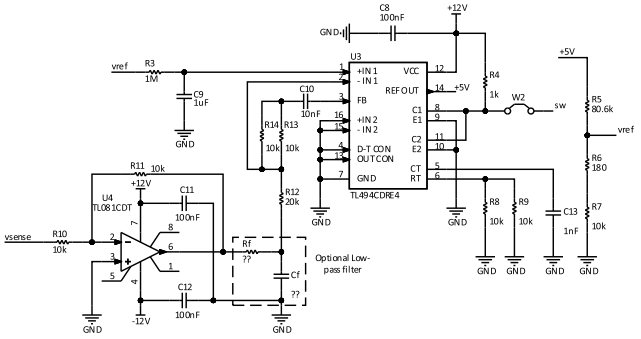

FIGURE 18. Control-stage.

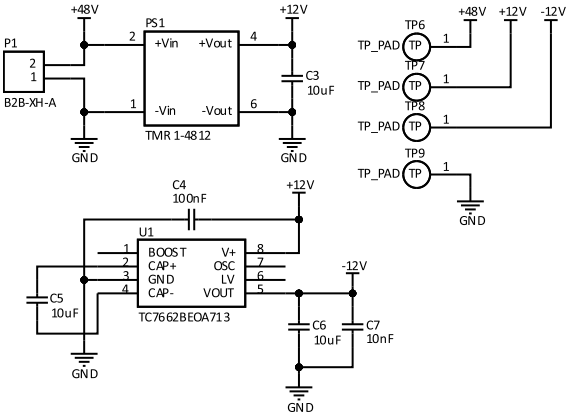

FIGURE 19. Power supply.

Finally, the transfer function needed to operate the Ćuk converter (for this application) under a closed-loop control scheme will be:

$$\frac{\hat{V}_{sense}(s)}{\hat{d}(s)} = \frac{R_{sense}}{R_o}\frac{\hat{V}_{C_2}(s)}{\hat{d}(s)} \tag{34}$$

where R_{sense} is the current-sense resistor (Fig. 2).

APPENDIX B
PEC SCHEMATIC

With the aim that this work can be reproduced by other researchers, the schematic diagram of the PEC is shown in this appendix. In Fig. 17, the power and driver stages are

depicted; Fig. 18 shows the control-stage implemented with a TL494; and finally, Fig. 19 shows the power supply of ±12 V.

ACKNOWLEDGMENT

The authors acknowledge all the anonymous people who fight *SARS-CoV-2* every day in their own area, which motivated them to put in their grain of salt during the pandemic. Francisco J. Perez-Pinal acknowledges his family support and resilience, which contracted and recovered from COVID-19 during this work.

REFERENCES

[1] W. Kowalski, "Introduction," in *Ultraviolet Germicidal Irradiation Handbook*, W. Kowalski, Ed. New York, NY, USA: Springer, 2009, ch. 1, pp. 1–16.

[2] W. Kowalski, "UVGI lamps and fixtures," in *Ultraviolet Germicidal Irradiation Handbook*, W. Kowalski, Ed. New York, NY, USA: Springer, 2009, ch. 5, pp. 119–137.

[3] W. Kowalski, "UVGI guidelines and standards," in *Ultraviolet Germicidal Irradiation Handbook*, W. Kowalski, Ed. New York, NY, USA: Springer, 2009, ch. 11, pp. 255–286.

[4] W. Kowalski, "UVGI deactivation theory," in *Ultraviolet Germicidal Irradiation Handbook*, W. Kowalski, Ed. New York, NY, USA: Springer, 2009, ch. 2, pp. 17–50.

[5] J. M. Alonso, E. Lopez, J. Ribas, A. J. Calleja, M. Rico-Secades, and J. Losada, "Design and implementation of an electronic ballast for UV-based ozone generation using a low cost microcontroller," in *Proc. IEEE 28th Annu. Conf. Ind. Electron. Soc. (IECON)*, Seville, Spain, vol. 1, Nov. 2002, pp. 383–388.

[6] S.-C. Wang and Y.-H. Liu, "High-power-factor electronic ballast with intelligent energy-saving control for ultraviolet drinking-water treatment systems," *IEEE Trans. Ind. Electron.*, vol. 55, no. 1, pp. 142–153, Jan. 2008.

[7] K. Erenturk, "Dynamic characterization of a UV fluorescent lamp," *IEEE Trans. Plasma Sci.*, vol. 36, no. 2, pp. 519–523, Apr. 2008.

[8] L. De Oro Arenas, G. E. de Azevedo e Melo, and C. A. Canesin, "Electronic ballast design for UV lamps based on UV dose, applied to drinking water purifier," *IEEE Trans. Ind. Electron.*, vol. 63, no. 8, pp. 4816–4825, Aug. 2016.

[9] X. Zhang, K. Dong, Y. Wang, D. Xu, and J. Jiang, "Research on the parameter optimization of electronic ballast for UV-lamps considering its lifetime and UVC irradiance," *IEEE Access*, vol. 6, pp. 11931–11939, 2018.

[10] S. Narla, A. B. Lyons, I. Kohli, A. E. Torres, A. Parks-Miller, D. M. Ozog, I. H. Hamzavi, and H. W. Lim, "The importance of the minimum dosage necessary for UVC decontamination of N95 respirators during the COVID-19 pandemic," *Photodermatol., Photoimmunol. Photomed.*, vol. 36, no. 4, pp. 324–325, Jul. 2020.

[11] K. O'Hearn, S. Gertsman, M. Sampson, R. Webster, A. Tsampalieros, R. Ng, J. Gibson, A. T. Lobos, N. Acharya, A. Agarwal, and S. Boggs, "Decontaminating N95 masks with ultraviolet germicidal irradiation (UVGI) does not impair mask efficacy and safety: A systematic review," in *Proc. OSF*, Mar. 2020, pp. 1–44.

[12] M. Bentancor and S. Vidal, "Programmable and low-cost ultraviolet room disinfection device," *HardwareX*, vol. 4, Oct. 2018, Art. no. e00046.

[13] K. J. Card *et al.*, "UV sterilization of personal protective equipment with idle laboratory biosafety cabinets during the Covid-19 pandemic," *medRxiv*, Oct. 2020, doi: 10.1101/2020.03.25.20043489.

[14] S. S. Nunayon, H. Zhang, and A. C. K. Lai, "Comparison of disinfection performance of UVC-LED and conventional upper-room UVGI systems," *Indoor Air*, vol. 30, no. 1, pp. 180–191, Jan. 2020.

[15] R. Kessler, "The minamata convention on mercury: A first step toward protecting future generations," *Environ. Health Perspect.*, vol. 121, no. 10, pp. A304–A309, Oct. 2013.

[16] C. Pernot, S. Fukahori, T. Inazu, T. Fujita, M. Kim, Y. Nagasawa, A. Hirano, M. Ippommatsu, M. Iwaya, S. Kamiyama, I. Akasaki, and H. Amano, "Development of high efficiency 255-355 nm AlGaN-based light-emitting diodes," *Phys. Status Solidi A*, vol. 208, no. 7, pp. 1594–1596, Jul. 2011.

[17] S. E. Beck, H. Ryu, L. A. Boczek, J. L. Cashdollar, K. M. Jeanis, J. S. Rosenblum, O. R. Lawal, and K. G. Linden, "Evaluating UV-C LED disinfection performance and investigating potential dual-wavelength synergy," *Water Res.*, vol. 109, pp. 207–216, Feb. 2017.

[18] K. Song, M. Mohseni, and F. Taghipour, "Application of ultraviolet light-emitting diodes (UV-LEDs) for water disinfection: A review," *Water Res.*, vol. 94, pp. 341–349, May 2016.

[19] Y. W. Lee, H. D. Yoon, J.-H. Park, and U.-C. Ryu, "Application of 265-nm UVC LED lighting to sterilization of typical gram negative and positive bacteria," *J. Korean Phys. Soc.*, vol. 72, no. 10, pp. 1174–1178, May 2018.

[20] T. Mathebula, F. W. Leuschner, and S. P. Chowdhury, "The use of UVC-LEDs for the disinfection of mycobacterium tuberculosis," in *Proc. IEEE PES/IAS PowerAfrica*, Cape Town, South Africa, Jun. 2018, pp. 739–744.

[21] D.-K. Kim and D.-H. Kang, "UVC LED irradiation effectively inactivates aerosolized viruses, bacteria, and fungi in a chamber-type air disinfection system," *Appl. Environ. Microbiol.*, vol. 84, no. 17, p. e00944-18, Sep. 2018.

[22] A. H.-T. Li, S. D. Chao, W.-C. Chen, and M.-F. Lin, "Wearable device system capable of effectively treating onychomycosis," in *Proc. Int. Automat. Control Conf. (CACS)*, Taoyuan, Taiwan, Nov. 2018, p. 1.

[23] T.-P. Sun, C.-T. Huang, P.-W. Lui, Y.-T. Chen, and H.-L. Shieh, "Novel measurement system for linear array type UVC germicidal system," in *Proc. IEEE Eurasia Conf. Biomed. Eng., Healthcare Sustainability (ECBIOS)*, Okinawa, Japan, May/Jun. 2019, pp. 57–60.

[24] P. O. Nyangaresi, Y. Qin, G. Chen, B. Zhang, Y. Lu, and L. Shen, "Comparison of the performance of pulsed and continuous UVC-LED irradiation in the inactivation of bacteria," *Water Res.*, vol. 157, pp. 218–227, Jun. 2019.

[25] L. Shen, T. M. Griffith, P. O. Nyangaresi, Y. Qin, X. Pang, G. Chen, M. Li, Y. Lu, and B. Zhang, "Efficacy of UVC-LED in water disinfection on bacillus species with consideration of antibiotic resistance issue," *J. Hazardous Mater.*, vol. 386, Mar. 2020, Art. no. 121968.

[26] M. Arias, A. Vázquez, and J. Sebastián, "An overview of the AC-DC and DC-DC converters for LED lighting applications," *Automatika*, vol. 53, no. 2, pp. 156–172, Jan. 2012.

[27] M. Forouzesh, Y. P. Siwakoti, S. A. Gorji, F. Blaabjerg, and B. Lehman, "Step-up DC-DC converters: A comprehensive review of voltage-boosting techniques, topologies, and applications," *IEEE Trans. Power Electron.*, vol. 32, no. 12, pp. 9143–9178, Dec. 2017.

[28] A. Gago-Calderón, R. D. Orejón-Sánchez, and M. J. Hermoso-Orzáez, "DC network indoor and outdoor LED lighting, light-emitting diode," in *Light-Emitting Diode—An Outlook on the Empirical Features and Its Recent Technological Advancements*, J. Thirumalai, Ed. London, U.K.: IntechOpen, 2018, ch. 2, pp. 405–414.

[29] N. T. Tung, N. D. Tuyen, N. M. Huy, N. H. Phong, N. C. Cuong, and L. M. Phuong, "Design and implementation of 150 W AC/DC LED driver with unity power factor, low THD, and dimming capability," *Electronics*, vol. 9, no. 1, p. 52, Jan. 2020.

[30] S. Ćuk and R. D. Middlebrook, "A new optimum topology switching DC-to-DC converter," in *Proc. IEEE Power Electron. Spec. Conf.*, Palo Alto, CA, USA, Jun. 1977, pp. 160–179.

[31] J. R. de Britto, A. E. Demian, L. C. de Freitas, V. J. Farias, E. A. A. Coelho, and J. B. Vieira, "A proposal of led lamp driver for universal input using cuk converter," in *Proc. IEEE Power Electron. Spec. Conf.*, Rhodes, Greece, Jun. 2008, pp. 2640–2644.

[32] SEOULVIOSYS. *UV CA3535 Series (CUD5GF1B)*. Accessed: Jul. 24, 2020. [Online]. Available: https://media.digikey.com/pdf/Data%20Sheets/Seoul%20Semiconductor/CUD5GF1B_R0.1_Prelliminary_2-3-20.pdf

[33] R. Erickson and D. Maksimovic, *Fundamentals of Power Electronics*, 2nd ed. New York, NY, USA: Springer, 2001.

[34] D. Mills, D. A. Harnish, C. Lawrence, M. Sandoval-Powers, and B. K. Heimbuch, "Ultraviolet germicidal irradiation of influenza-contaminated N95 filtering facepiece respirators," *Amer. J. Infection Control*, vol. 46, no. 7, pp. e49–e55, Jul. 2018.

[35] Physics World. (Jun. 16, 2020). *Microbe-Killing Short-Wavelength UV Radiation Produced by LEDs*. Accessed: Jun. 29, 2020. [Online]. Available: https://physicsworld.com/a/microbe-killing-short-wavelength-uv-radiation-produced-by-leds/

[36] M. Buonanno, D. Welch, I. Shuryak, and D. J. Brenner, "Far-UVC light (222 nm) efficiently and safely inactivates airborne human coronaviruses," *Sci. Rep.*, vol. 10, no. 1, Jun. 2020, Art. no. 1.

[37] H. Inagaki, A. Saito, H. Sugiyama, T. Okabayashi, and S. Fujimoto, "Rapid inactivation of SARS-CoV-2 with deep-UV LED irradiation," *Emerg. Microbes Infections*, vol. 9, no. 1, p. 1747, Jul. 2020.

[38] Boston Electronics. *Ultraviolet Light Emitting Diodes (UV LED)*. Accessed: Jul. 24, 2020. [Online]. Available: https://www.boselec.com/wp-content/uploads/Linear/Nikkiso/UV-LED-Catalog-06-18-19.pdf
[39] A. Rezaie, G. G. S. Leite, G. Y. Melmed, R. Mathur, M. J. Villanueva-Millan, G. Parodi, J. Sin, J. F. Germano, W. Morales, S. Weitsman, S. Y. Kim, J. H. Park, S. Sakhaie, and M. Pimentel, "Ultraviolet a light effectively reduces bacteria and viruses including coronavirus," *PLoS ONE*, vol. 15, no. 7, Jul. 2020, Art. no. e0236199.
[40] SEOULVIOSYS. *UV AAP Series (CUD4AF1B)*. Accessed: Jul. 24, 2020. [Online]. Available: https://www.neumueller.com/datenblatt/seoulviosys/CUD4AF1B_200410_R0.7_Preliminary.pdf
[41] R. D. Middlebrook and S. Ćuk, "A general unified approach to modelling switching-converter power stages," in *Proc. IEEE Power Electron. Spec. Conf.*, Cleveland, OH, USA, Jun. 1976, pp. 18–34.

FRANCISCO A. JUAREZ-LEON received the B.S. degree in electronics engineering from the Technological Institute of Celaya, Mexico, in 2017, where he is currently pursuing the M.Sc. degree in electronics engineering with a specialization in power electronics. He has collaborated twice on research projects with the Gijón Polytechnic School of Engineering/University of Oviedo, Spain. His research interests include power conversion, mathematical modeling of power converters, control theory applied to power electronics, and advanced digital systems.

ALLAN GIOVANNI SORIANO-SÁNCHEZ received the degree in electronics and automation engineering from the Autonomous University of Nuevo Leon (UANL), in 2011, and the M.Sc. degree in electrical engineering with an orientation in automatic control and the Ph.D. degree in electrical engineering from the Faculty of Mechanical and Electrical Engineering, UANL, in 2013 and 2016, respectively. His research interests include chaos systems, nonlinear control, and power electronic converters.

MARTÍN A. RODRÍGUEZ-LICEA received the Ph.D. degree in applied sciences in the option of control and dynamic systems from the Instituto Potosino de Investigación Científica y Tecnológica. He has been a CONACYT Professor assigned to the Instituto Tecnológico de Celaya and a member of the National System of Researchers Level C, since 2017. His research interests include nonlinear systems and power electronic converters.

FRANCISCO J. PEREZ-PINAL (Senior Member, IEEE) received the M.Sc. degree in electrical engineering jointly from the University of Birmingham, Birmingham, U.K., and the University of Nottingham, Nottingham, U.K., in 2002, and the Ph.D. degree in electrical engineering from the Autonomous University of San Luis Potosí, San Luis Potosí, Mexico, in 2008. He is currently a Professor with the Department of Electronic Engineering, Instituto Tecnológico de Celaya, Celaya, Mexico. His research interests include power electronics, energy conversion systems, and transportation electrification.